Pergamon

Cement and Concrete Research 31 (2001) 1887–1893

CEMENT AND CONCRETE RESEARCH

Nuclear magnetic resonance characterization of high- and ultrahigh-performance concrete Application to the study of water leaching

Charlotte Porteneuve[a,*], Hélène Zanni[a], Christian Vernet[b], Knut O. Kjellsen[c], Jean-Pierre Korb[d], Dominique Petit[d]

[a]*Laboratoire de Physique et Mécanique des Milieux Hétérogènes, UMR CNRS 7636, Ecole Supérieure de Physique et Chimie Industrielles, 10 rue Vauquelin, 75231 Paris Cedex 05, France*

[b]*LAFARGE-LCR, 95 rue Montmurier BP15, 38291 Saint Quentin Fallavier Cedex, France*

[c]*R&D Department, NORCEM AS, N-3950 Brevik, Norway*

[d]*Laboratoire de Physique de la Matière Condensée, UMR CNRS 7643, Ecole Polytechnique, 91128 Palaiseau, France*

Received 16 January 2001; received in revised form 7 August 2001

Abstract

In the present study, we show that high-resolution ^{29}Si and ^{27}Al magic angle spinning (MAS) nuclear magnetic resonance (NMR) can be a powerful tool for analyzing actual concrete mixes. The influence of the amount of silica fume and of the type of cement in high-performance concrete (HPC), as well as the influence of the type of silica fume and of the granular packing in ultrahigh-performance concrete (UHPC) were investigated. Significant effects on the amount and shape of C-S-H, on the incorporation of aluminum in the C-S-H structure, and on the distribution of aluminum-containing hydrates were observed. Nuclear magnetic relaxation of protons was also performed and it showed the fractal feature of the pore size distribution in UHPC and the higher amount of larger pores in HPC. The microstructure of the surface of these same formulations leached by mineral water for up to 1 year exhibits slight modifications.

Keywords: High-performance concrete; Microstructure; Pore size distribution; Degradation; Nuclear magnetic resonance

1. Introduction

The recent improvements of concrete mechanical properties and compactness through the optimization of the granular packing and through the adjustment of pozzolans and other admixtures [1] has made this material a candidate for the storage of nuclear wastes deep underground, in a potentially humid environment. Still, its physical–chemical behavior is not yet fully understood. Nuclear magnetic resonance (NMR) spectroscopy has been widely used for almost two decades to investigate the microstructure of cement-based materials because of its suitability to crystalline as well as to amorphous materials. ^{29}Si magic angle spinning (MAS) NMR experiments provide quantitative information on the fractions of silicon present in different tetrahedral environments in silicates [2,3]. Similarly, although it exhibits electric quadrupole interactions, making the interpretation of the spectra more difficult, ^{27}Al MAS NMR has proven to be helpful for the study of aluminum in this type of materials, for instance as guest ions [4] or for the transformation of ettringite into monosulfate [5]. Concrete porosity has also been studied by ^{1}H [6–8] magnetization relaxation, which is sensitive to the dynamics of water molecules into the pore structure. This nondestructive technique hence allows investigation of both open and closed porosity and revealed the hierarchical discrete pore size distribution in reactive powder concrete recently [8–10].

In the present study, the effect of formulation parameters on the microstructure and microporosity of high-performance concrete (HPC) and ultrahigh-performance concrete (UHPC) has been investigated by ^{29}Si and ^{27}Al MAS NMR and by ^{1}H magnetization relaxation. Special attention was put on the granular packing, on the reactivity

* Corresponding author. Tel.: +33-1-40-79-45-56; fax: +33-1-40-79-47-95.

E-mail addresses: charlie@pmmh.espci.fr; charlotte.porteneuve@free.fr (C. Porteneuve).

0008-8846/01/$ – see front matter
PII: S0008-8846(01)00648-2

of silica fume, and on the composition of cement. The concrete samples were then submitted to a water leaching test as representative as possible to actual leaching conditions for up to 1 year. The evolution of their microstructure was investigated by solid-state NMR throughout leaching time.

2. Methods

2.1. Samples

The specific characteristics of HPC and UHPC formulations are given in Tables 1 and 2, respectively. The influence of the amount of silica fume and of the type of cement has been considered for HPC. In the case of UHPC, the filling ratio and the chemical reactivity of silica fume, embodied by its BET surface, have been studied. The former is equal to the ratio of the volume occupied by the fine particles in between the cement grains and the theoretical volume of voids in a dense packing of cement grains. The higher the filling ratio, the higher is the silica fume content, and the least compact is the cement grains packing. The NMR characterization was performed on ground 3-month-old nonleached samples. The second set of experiments was performed on the same six formulations leached up to 1 year. The corresponding nonleached reference samples were also studied in order to take the aging effect into account.

2.2. Water leaching test

For each formulation of concrete, the leaching test consists of mineral water continuously flowing at a rate of 7 ml/h between 6-mm-thick concrete disks, with a constant renewal of the leaching water. Every 3 months up to 1 year, one disk was removed from the apparatus and then 1 mm of its surface was selected using a diamond saw, in order to prevent contamination of the sample. According to scanning electronic microscopy, the depth of alteration reaches 100 μm for all six mixes, so that only a low percentage of each sample studied by NMR is actually made up of leached material.

Table 1
Characteristics of HPC mixes: weight ratios in term of cement mass

Components	20% silica fume	5% silica fume	5% silica fume, fly ash cement
Cement	1.00	1.00	1.00 fly ash cement
Silica fume	0.20	0.50	0.50
Limestone aggregates	3.79	3.27	3.41
Water	0.34	0.29	0.29

The samples were mixed and cured at 20 °C. The cement used contains 22.7% SiO_2 and 4.3% Fe_2O_3. The fly ash cement contains 25.2% SiO_2 and 4.4% Fe_2O_3.

Table 2
Characteristics of UHPC mixes: weight ratios in term of cement mass

Components	C_1 filling ratio	C_2 filling ratio	C_1 filling ratio
Cement	1.000	1.000	1.000
Silica fume	0.325 (12 m^2/g BET)	0.150 (12 m^2/g BET)	0.325 (21.5 m^2/g BET)
Crushed quartz	0.300	0.150	0.300
Sand	1.430	2.000	1.430
Water	0.200	0.240	0.240

The samples were mixed at 20 °C and cured at 90 °C during 48 h after demolding. The filling ratios C_1 and C_2 are 2.2 and 1.1, respectively. The cement used contains 22.7% SiO_2 and 4.3% Fe_2O_3.

2.3. Nuclear magnetic resonance

High-resolution solid-state ^{29}Si and ^{27}Al MAS—spinning of the sample about an axis at 54.7° relative to the magnetic field direction—NMR spectra were recorded at 99.4 and 130.3 MHz, respectively, on a Bruker ASX500 (11.7 T) spectrometer.

^{29}Si MAS NMR experiments were recorded using a CPMAS probe with 7-mm zirconium oxide rotors spinning at $\nu_r = 7$ kHz. Ninety-degree single-pulse experiments were performed with 30-s pulse recycle delay. The ^{29}Si isotropic chemical shift of the peaks were analyzed using the Q^n classification [3,11], where Q stands for SiO_4 tetrahedron and *n* refers to the number of tetrahedra linked by oxygen bonds to the latter tetrahedron. Q^0 species are encountered in cement while Q^4 are encountered in silica fume, sand, and crushed quartz. Q^1 and Q^2 are end- and middle-chain SiO_4 tetrahedra, respectively, in C-S-H. ^{29}Si chemical shifts are referenced to external trimethylsilyl ester of cubic octameric silicate Q_8M_8.

^{27}Al MAS NMR experiments were recorded using a CPMAS probe with 4-mm zirconium oxide rotors spinning at $\nu_r = 12$kHz. Fifteen-degree single-pulse excitations with pulse widths below 1 μs were performed with 1-s delay,

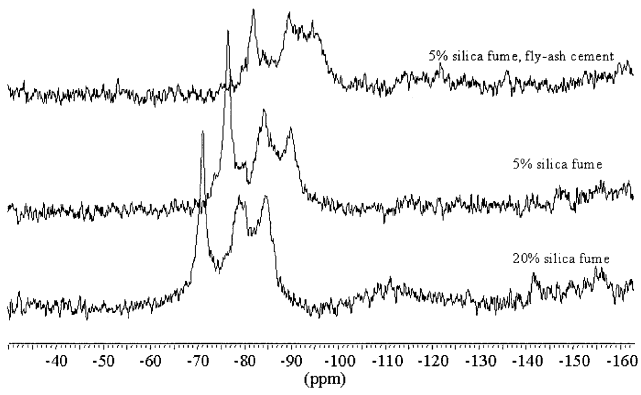

Fig. 1. ^{29}Si MAS NMR spectra of the three HPC formulations hydrated for 3 months recorded at 11.7 T using a spinning speed of $\nu_r = 7$ kHz, a recycle time of 30 s, and 1000 scans.

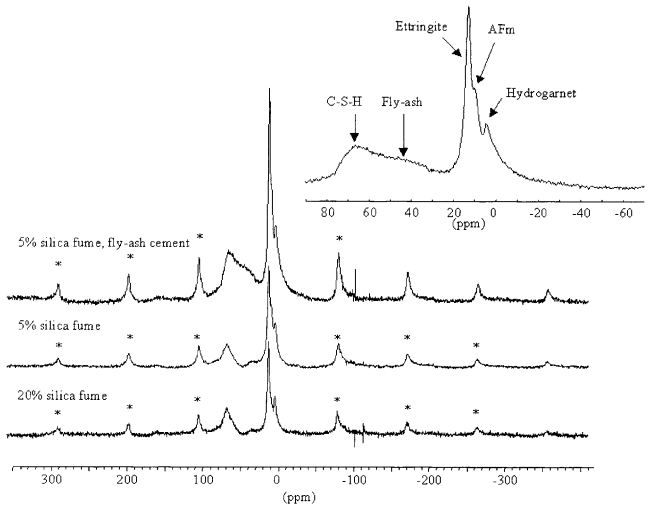

Fig. 2. ^{27}Al MAS NMR spectra of the three HPC formulations hydrated for 3 months recorded at 11.7 T using a spinning speed of $\nu_r = 12$ kHz, a recycle time of 1 s and 10,000 scans. The asterisks indicate spinning side bands of the central band of ettringite.

ensuring a quantitative distribution of the peaks integrated intensity. ^{27}Al chemical shifts are referenced to external 1.0 M $AlCl_3-6H_2O$.

The isotropic chemical shift difference of about 60 ppm between tetrahedrally and octahedrally coordinated aluminum, in addition to the knowledge of the quadrupole coupling parameters (i.e., the quadrupole coupling constant, C_Q, and asymmetry parameter η, $0 \leq \eta \leq 1$, of the electric field gradient tensor) usually allows the assessment of the peaks [4,5,12]. A preliminary study of the anhydrous and other possible aluminum-containing hydrate phases in concrete also contributed to the sorting of the different peaks (spectra not shown). In particular, aluminum substituted to

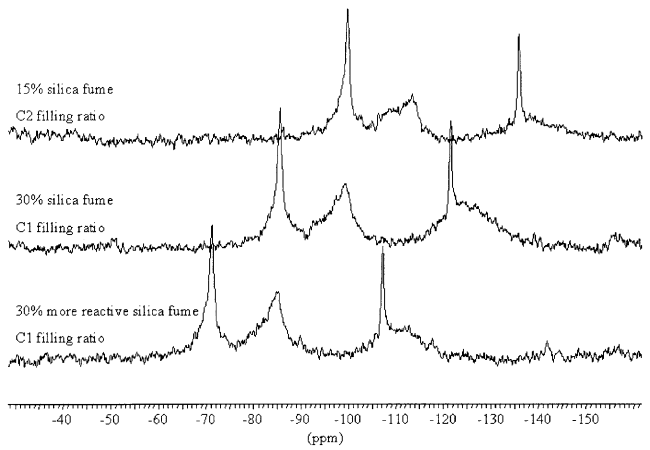

Fig. 3. ^{29}Si MAS NMR spectra of the three UHPC formulations hydrated for 3 months recorded at 11.7 T using a spinning speed of $\nu_r = 7$ kHz, a recycle time of 30 s, and 1000 scans.

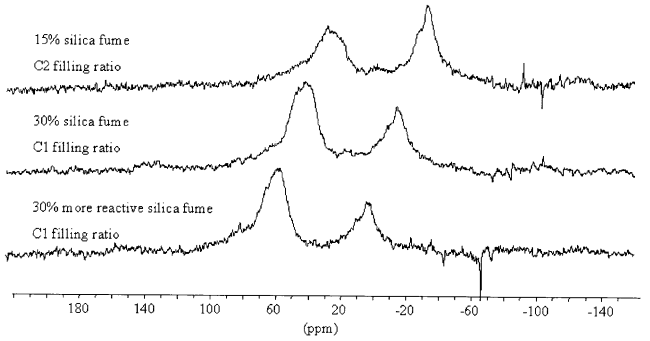

Fig. 4. ^{27}Al MAS NMR spectra of the three UHPC formulations hydrated for 3 months recorded at 11.7 T using a spinning speed of $\nu_r = 12$ kHz, a recycle time of 1 s, and 10,000 scans.

silicon in the C-S-H structure in tetrahedral coordination and aluminum from ettringite and monosulfate in octahedral coordination were identified.

Measurement of the longitudinal proton magnetization decay was performed through the inversion recovery method at 300 MHz in static conditions at room temperature on all six nonleached concrete samples. The nonexponential decay observed as in previous studies on similar materials [8–10] was fitted to a weighted sum of five well-resolved single exponential functions. The deduced relaxation times spread over five orders of magnitude and their frequency dependence also observed in a previous study [8]

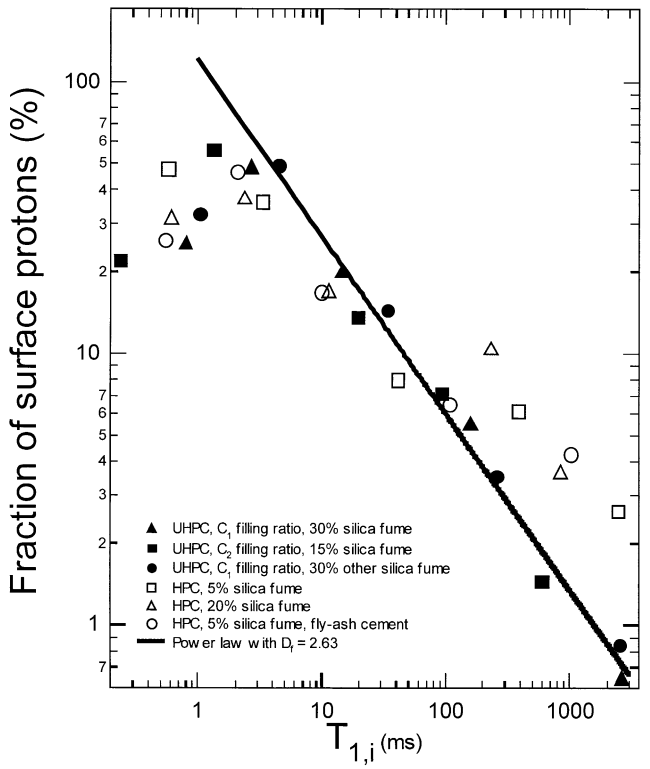

Fig. 5. Fraction of surface protons vs. longitudinal relaxation time T_1 for all six HPC and UHPC formulations.

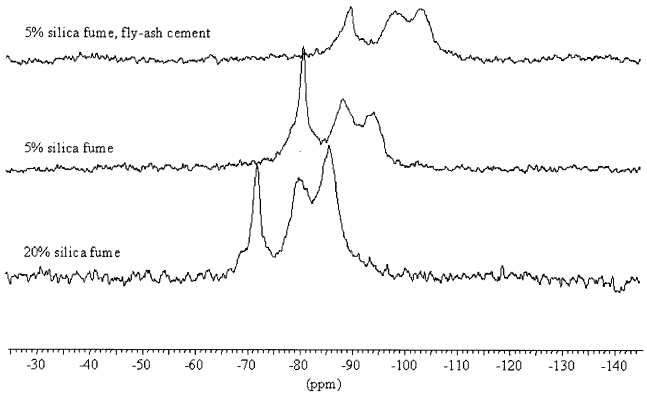

Fig. 6. ^{29}Si MAS NMR spectra of the three HPC formulations leached for 1 year recorded at 11.7 T using a spinning speed of $\nu_r = 7$ kHz, a recycle time of 30 s, and 1000 scans.

validate the biphasic fast exchange model. Protons relax through hydrated paramagnetic ions present at the surface of the pores. Assuming a spherical pore shape, the latter model (Eq. (1)) allows a linear relationship between the i-th spin-lattice relaxation time $T_{1,i}$ and the i-th average pore size $\langle R\rangle_i$ [8]:

$$\langle R\rangle_i = (30 N_s v_{solv} H_I{}^2 n T_{1e}) T_{1,i} \quad (1)$$

where N_s is the surface density of paramagnetic spins, v_{solv} is the volume of the solvation cage made by the paramagnetic impurity and the water molecules interacting with it, H_I is the dipole–dipole coupling between the paramagnetic spin S (Fe^{3+} ions) and the proton spin I, n is the average number of water molecules in the volume v_{solv}, and T_{1e} is the electron spin-lattice relaxation time of Fe^{3+} ions. Consequently, the distribution of average pore radii $\langle R\rangle_i$ is similar to the one of relaxation times $T_{1,i}$.

3. Results

3.1. Characterization of nonleached samples

3.1.1. High-performance concrete

The ^{29}Si MAS NMR spectra of the three HPC mixes hydrated for 3 months are presented in Fig. 1. Q^0 species of remaining cement display a maximum intensity at -71 ppm, while C-S-H are observed in the Q^1 and Q^2 regions at -79 and -85 ppm, respectively. The peaks respective integrated intensity and the Q^2/Q^1 ratio show that a higher amount of silica fume increases the amount of precipitated C-S-H as well as their silicate chain length, as was already shown [13–16]. The amount of hydrates relative to remaining cement in the case of fly ash cement is more important. However, the C-S-H chain length does not appear to vary when cement is replaced by fly ash cement, after 3 months of hydration.

The ^{27}Al MAS NMR results, presented on Fig. 2, show the broad contribution at around 50 ppm of fly ash between the tetrahedral and octahedral chemical shift area. However, the intensity of the other peaks does not appear to be much affected by the formulation parameters. The three main octahedral center band contributions are identified as ettringite, AFm, and hydrogarnet with decreasing frequency, respectively. We note that ettringite is at the origin of most of the observed spinning side bands. The peak observed in tetrahedral coordination differs from the one of anhydrous cement, which is overwhelmed by the one of Al guest ions in calcium silicates (spectrum not shown) [5]. The absence of any spectral features corresponding to calcium aluminate phase is ascribed to its strong quadrupole couplings, which result in line broadening. Furthermore, ferrite phase C_4AF is difficult to detect by ^{27}Al MAS NMR because of its high Fe^{3+} content. Several studies [5,17] have shown that aluminum ions substituted in calcium silicates preferably remain in these phases instead of participating to the precipitation of hydration products like ettringite or monosulfate. The asymmetric center band ranging from 80 to 30 ppm was thus attributed to aluminum substituted to silicon in the C-S-H.

3.1.2. Ultrahigh-performance concrete

^{29}Si MAS NMR shows for UHPC that the filling ratio influences the amount and shape of precipitated C-S-H as can be seen in Fig. 3. In addition to the peaks observed for HPC, UHPC shows a narrow line overlapping the one of silica fume at -107 ppm, which corresponds to crushed quartz and sand. As in HPC, a higher amount of silica fume increases the precipitation of C-S-H, as well as their silicate chain length. We note that after 3 months of hydration, silica fume still remains in all UHPC samples. Consequently, the C-S-H chain length is mostly governed by the availability of initial silica fume, which is determined by the filling ratio in UHPC. However, the BET surface area difference between the two silica fumes does not appear to have as much effect

Table 3
Amount of silicate species expressed in percentage and deduced from the decomposition of ^{29}Si NMR spectra of the three HPC mixes leached for 1 year

	20% silica fume		5% silica fume		5% silica fume, fly ash cement	
	Nonleached	12 months leaching	Nonleached	12 months leaching	Nonleached	12 months leaching
Cement Q^0	30	22	36	36	41	36
C-S-H (Q^1+Q^2)	66	67	64	64	54	64
Silica fume (Q^4)	5	0	0	0	6	0
Q^3 species	0	11	0	0	0	0

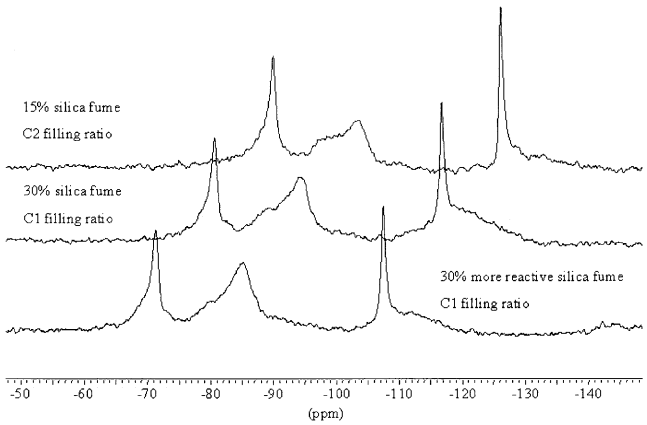

Fig. 7. ^{29}Si MAS NMR spectra of the three UHPC formulations leached for 1 year recorded at 11.7 T using a spinning speed of $\nu_r = 7$ kHz, a recycle time of 30 s, and 1000 scans.

as the filling ratio on the C-S-H precipitation. The consumption of silica fume is slightly more important when it is more reactive.

^{27}Al MAS NMR spectra of the three UHPC mixes are displayed in Fig. 4. They present very similar features, except for the tetrahedral contribution corresponding to aluminum substituted to silicon in the C-S-H structure. It is indeed more intense when there is more silica fume, which may be related to the fact that aluminum preferably substitutes middle-chain tetrahedra in the C-S-H [12,17]. If C-S-H has longer chains, which is the case for C_1 filling ratio formulations, then the probability of substitution is higher. We can also note the quasi-absence of spinning side bands on UHPC ^{27}Al NMR spectra compared to HPC, which is mostly related to the lesser contribution of ettringite.

3.1.3. Porosity features

In addition to the microstructure, we investigated the porosity features of all nonleached samples by ^{1}H NMR. The fraction of protons—expressed in percentage—as a function of longitudinal relaxation time for all HPC and UHPC samples is displayed in Fig. 5. Except for the smaller pores, the UHPC distribution of average pore sizes $\langle R \rangle_i$ follows a power law, regardless of the formulation. This type of law is also expected in the computation of the total surface area $S_{\text{total}}(i)$ for each pore category $\langle R \rangle_i$ in a hierarchical distribution of noncommunicating or badly communicating spherical pores (Eq. (2)):

$$S_{\text{total}}(i) \propto \langle R \rangle_i^{2-D_f} \tag{2}$$

where D_f is the surface fractal dimensionality ($2 \leq D_f \leq 3$). The slope of the power laws found for UHPC then give access to the value of D_f, which ranges around 2.6.

On the contrary, HPC average pore size distribution does not exhibit such a hierarchy over several orders of magnitude. It also differs from UHPCs in the larger pore size range, which is, as expected, more important for HPC due to the larger part of capillary porosity. The fractal feature of UHPC pore size distribution can then be interpreted as a consequence of the quasi-fractal feature of the granular packing in this type of concrete. Meanwhile, the smaller relaxation times are always in the same range, regardless of the type of concrete or of the power law. They are likely to correspond to C-S-H bricks' intrinsic porosity. A previous study on similar materials [9] indeed gave 7 Å for the smaller accessible pore size with this method.

3.2. Leaching of high- and ultrahigh-performance concrete

3.2.1. High-performance concrete

^{29}Si MAS NMR spectra of the three HPC mixes leached up to 1 year are displayed in Fig. 6 and their decomposition is presented on Table 3. A systematic comparison with reference samples was performed in order to differentiate the aging effect from the leaching effect. Most HPC formulations do not exhibit much microstructure modifications, except for the formulation with 20% silica fume, which shows a slight precipitation of Q^3 at -92 ppm. Moreover, the ratio of precipitated C-S-H over the remaining cement increases with leaching, especially when there are more pozzolans. We note that this ratio is more important when there is more silica fume, regardless of the leaching. However, the mix containing fly ash exhibits longer C-S-H chains than the formulation with only 5% of silica fume after 1 year of leaching. A comparison with the ^{29}Si NMR spectra of the same samples leached for 3 months shows the increase of the average C-S-H chain length in all formulations as a consequence of aging.

^{27}Al MAS NMR did not show any significant effect of leaching or aging up to 1 year.

Table 4
Amount of silicate species expressed in percentage and deduced from the decomposition of ^{29}Si NMR spectra of the three UHPC mixes leached for 1 year

	C_2 filling ratio, 15% silica fume		C_1 filling ratio, 30% silica fume		C_1 filling ratio, 30% more reactive silica fume	
	Nonleached	12 months leaching	Nonleached	12 months leaching	Nonleached	12 months leaching
Cement Q^0	43	42	29	24	33	28
C-S-H ($Q^1 + Q^2$)	36	44	34	40	35	46
Silica fume (Q^4)	21	14	37	33	30	17
Q^3 species	0	0	0	3	3	9

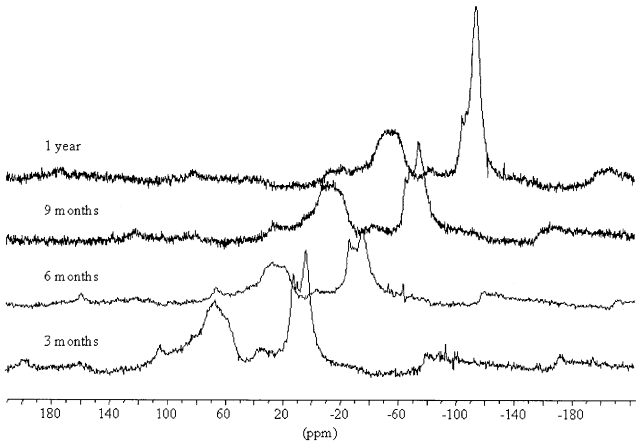

Fig. 8. ^{27}Al MAS NMR spectra of the UHPC formulation with 15% silica fume leached from 3 months up to 1 year, recorded at 11.7 T using a spinning speed of $\nu_r = 12$ kHz, a recycle time of 1 s, and 10,000 scans.

3.2.2. Ultrahigh-performance concrete

As for HPC, UHPC samples do not show very significant microstructure modifications up to 1 year of leaching. Their ^{29}Si MAS NMR spectra are displayed in Fig. 7. A quite similar pattern as after 3 months of hydration between the three mixes can be observed. Still, the decomposition given in Table 4 shows that the silica fume with the higher BET surface area is more consumed than the other one, especially in leaching conditions. The ratio of precipitated C-S-H over remaining cement increases for all UHPC formulations. Leaching then acts as a rehydration promoter: the dissolution of cement grains induces the precipitation of new C-S-H and portlandite, which reacts with the available silica fume and forms more C-S-H. Q^3 species also appear in small amounts at -92 ppm as a consequence of leaching in the formulations with the higher silica fume content.

^{27}Al NMR does not show major modifications of leached UHPC spectra except for the formulation with 15% silica fume, as can be seen in Fig. 8. After 3 months of leaching, the ettringite peak contribution increases compared to the nonleached sample after 3 months of hydration. The ettringite peak then decreases, while the hydrogarnet peak increases. The center band from gibbsite AH_3 has an isotropic chemical shift at 1 ppm close to the one of hydrogarnet so it may also contribute to the peak. This effect has been referred to as matrix effect [18]: aluminum-containing phases dissolve faster than hydrogarnet and/or gibbsite AH_3, which consequently exhibits a more important contribution on ^{27}Al MAS NMR spectra with leaching time.

4. Summary

This high-resolution solid-state NMR study has shown how this technique could provide information on actual HPC and UHPC formulations. The amount and average chain length of the C-S-H in HPC and UHPC increases when the initial amount of silica fume and/or fly ash is higher. The proportion of aluminum substituted to silicon in the C-S-H compared to other aluminum-containing hydrates is more important in UHPC. A correlation was established between the degree of substitution and the average chain length, namely, the number of middle-chain tetrahedra available for substitution. The distribution of aluminum-containing hydrates is different between HPC and UHPC: ettringite overwhelms in the former, while AFm contribution is more important in the latter.

The porosity features investigated by ^{1}H nuclear magnetization relaxation are also different in the hierarchy of the pore size distribution. UHPC shows an almost fractal distribution with a surface fractal dimension at around 2.6. Although HPC exhibits the same features as UHPC for the smaller pores, the proportion of larger pores is higher.

After 1 year of mineral water leaching, the microstructure of both types of concrete has not changed significantly. Still, we observed that leaching enhances the dissolution of cement and hence the precipitation of C-S-H, as well as the pozzolanic reaction according to the amount of remaining silica fume. A high amount of silica fume also appears to promote the slight precipitation of Q^3 species. In one case of UHPC, ^{27}Al NMR showed the faster dissolution of aluminum-containing phases relative to hydrogarnet and/or gibbsite.

Acknowledgments

We thank the European Community for the financial support in the Brite-Euram BE97-4452 UNICORN Research Project.

References

[1] P. Richard, M. Cheyrezy, Composition of reactive powder concretes, Cem. Concr. Res. 25 (1995) 1501–1511.
[2] E. Lippmaa, M. Mägi, M. Tarmak, W. Wieker, A.R. Grimmer, A high resolution ^{29}Si NMR study of the hydration of tricalcium silicate, Cem. Concr. Res. 12 (1982) 597–602.
[3] G. Engelhardt, D. Michel, High-Resolution Solid-State NMR of Silicates and Zeolites, Wiley, Chichester, 1987.
[4] S. Komarneni, R. Roy, D.M. Roy, C.A. Fyfe, G.J. Kennedy, Al-substituted tobermorite—the coordination of aluminum as revealed by solid-state ^{27}Al magic angle spinning (MAS) NMR, Cem. Concr. Res. 15 (1985) 723–728.
[5] J. Skibsted, J. Jakobsen, Characterization of the calcium silicate and aluminate phases in anhydrous and hydrated Portland cements by ^{27}Al and ^{29}Si MAS NMR spectroscopy, in: P. Colombet, A.-R. Grimmer, H. Zanni, P. Sozzani (Eds.), Nuclear Magnetic Resonance Spectroscopy of Cement-Based Materials, Springer-Verlag, Berlin, 1998, pp. 3–45.
[6] E.W. Hansen, H.C. Gran, P.O. Kvernberg, B. Pedersen, Surface-to-volume ratio of porous materials obtained by a combined use of NMR and MIT, J. Phys. Chem. B 101 (1997) 9206–9214.
[7] J. Greener, H. Peemoeller, R. Changho Choi, R. Holly, E. Reardon, C.M. Hansson, M.M. Pintar, Monitoring of hydration of white cement

paste with proton NMR spin–spin relaxation, J. Am. Ceram. Soc. 83 (3) (2000) 623–627.
[8] J.-P. Korb, D. Petit, S. Philippot, H. Zanni, V. Marret, M. Cheyrezy, Nuclear relaxation of water confined in reactive powder concrete, in: P. Colombet, A.-R. Grimmer, H. Zanni, P. Sozzani (Eds.), Nuclear Magnetic Resonance Spectroscopy of Cement-Based Materials, Springer-Verlag, Berlin, 1998, pp. 333–343.
[9] S. Philippot, J.-P. Korb, D. Petit, G. Counio, H. Zanni, Analysis of microporosity of reactive powder concrete by proton nuclear relaxation, J. Chim. Phys. 95 (1998) 332–336.
[10] S. Philippot, J.-P. Korb, D. Petit, H. Zanni, Analysis of microporosity and setting of reactive powder concrete by proton nuclear relaxation, Magn. Reson. Imaging 16 (5/6) (1998) 515–519.
[11] I. Klur, B. Pollet, J. Virlet, A. Nonat, C-S-H structure evolution with calcium content by multinuclear NMR, in: P. Colombet, A.-R. Grimmer, H. Zanni, P. Sozzani (Eds.), Nuclear Magnetic Resonance Spectroscopy of Cement-Based Materials, Springer-Verlag, Berlin, 1998, pp. 119–141.
[12] P. Faucon, T. Charpentier, D. Bertrandie, A. Nonat, J. Virlet, J.C. Petit, Characterization of calcium aluminate hydrates and related hydrates of cement pastes by ^{27}Al MQ-MAS NMR, Inorg. Chem. 37 (1998) 3726–3733.
[13] J. Skibsted, High-speed ^{29}Si and ^{27}Al MAS NMR studies of Portland and high alumina cements, Geopolymer, (1988) 179–196.
[14] C.M. Dobson, D.G.C. Goverdhan, J.D.F. Ramsay, S.A. Rodger, ^{29}Si MAS NMR study of the hydration of tricalcium silicate in the presence of finely divided silica, J. Mater. Sci. 23 (1988) 3–8.
[15] H. Justnes, I. Meland, J.O. Bjoergum, J. Krane, A ^{29}Si MAS NMR study of the pozzolanic activity of condensed silica fume and the hydration of di- and tricalcium silicates, Adv. Cem. Res. 3 (1990) 789–798.
[16] H. Zanni, M. Cheyrezy, V. Marret, S. Philippot, P. Nieto, Investigation of hydration and pozzolanic reaction in reactive powder concrete (RPC) using ^{29}Si NMR, Cem. Concr. Res. 26 (1) (1996) 93–100.
[17] I.G. Richardson, A.R. Brough, R. Brydson, G.W. Groves, C.M. Dobson, Location of aluminum in substituted calcium silicate hydrate (C-S-H) gels as determined by Si and Al NMR and EELS, J. Am. Ceram. Soc. 76 (1993) 2285–2288.
[18] P. Faucon, J.F. Jacquinot, F. Adenot, N. Gautier, D. Massiot, J. Virlet, ^{27}Al MAS NMR study on cement paste degradation by water, in: P. Colombet, A.-R. Grimmer, H. Zanni, P. Sozzani (Eds.), Nuclear Magnetic Resonance Spectroscopy of Cement-Based Materials, Springer-Verlag, Berlin, 1998, pp. 403–409.